A NEW DESIGN-ORIENTED MODEL OF GFRP REINFORCED HOLLOW CONCRETE COLUMNS

Omar S. AlAjarmeh, Allan C. Manalo, Brahim Benmokrane, Karu Karunasena, Wahid Ferdous, and Priyan Mendis

Biographies

Omar S. AlAjarmeh is a PhD Candidate at the School of Civil Engineering and Surveying in the University of Southern Queensland (USQ), Australia. He received his BS from Tafila Technical University (TTU), Jordan and MEng from the University of Jordan (UJ), Jordan.

Allan C. Manalo is an Associate Professor at the School of Civil Engineering and Surveying and the leader of the Civil Composites Research Group at USQ. He is a member of Engineers Australia and the Concrete Institute of Australia. His research interests include engineered composite materials and structures, polymer railway sleepers, and structural testing.

Brahim Benmokrane, **FACI**, is Professor of Civil Engineering and NSERC Research Chair in FRP Reinforcement for Concrete Infrastructure and Tier-1 Canada Research Chair in Advanced Composite Materials for Civil Structures in the Department of Civil Engineering at the University of Sherbrooke, Sherbrooke, QC, Canada. He is a member of ACI Committee 440 FRP Reinforcement and serves as co-chair of Canadian Standard Association (CSA) committees on FRP structural reinforcing materials for building design code (CSA S806) and the Canadian Highway Bridge Design Code (CSA S6). He is the founding chair of CSA technical committees S807 and S808 on specifications for FRP reinforcement.

Warna Karunasena is a Professor at the School of Civil Engineering and Surveying, USQ. He is a member of Engineers Australia, ASCE, and Structural Engineering Institute-USA. His research interests include composite materials, and modelling and analysis of structures.

Wahid Ferdous is a research fellow at USQ. He is a member of Engineers Australia. His research interests include engineered composite structures and polymer railway sleepers.

Priyan Mendis is a Professor in the Department of Infrastructure Engineering and the Leader of the Advanced Protective Technology of Engineering Structures Group in the University of Melbourne, Australia. He is a member of ACI, Concrete Institute of Australia, and Engineers Australia. His research interests include fire behavior of structures, high-strength concrete, and modeling and durability of infrastructure.

ABSTRACT

Hollow concrete columns (HCCs) reinforced with glass-fiber-reinforced-polymer (GFRP) bars and spirals are considered an effective design solution for bridge piers, electric poles, and ground piles because they use less material and maximize the strength-to-weight ratio. HCC behavior is affected by critical design parameters such as inner-to-outer diameter ratio, reinforcement and volumetric ratios, and concrete compressive strength. This paper proposes a new design-oriented model based on the plasticity theory of concrete and considering the critical design parameters to accurately describe the compressive load–strain behavior of GFRP-reinforced HCCs under monotonic and concentric loading. The validity of the proposed model was evaluated against experimental test results for 14 full-scale hollow concrete columns reinforced with GFRP bars and spirals. The results demonstrated that the proposed design-oriented model was accurate and yielding a very good agreement with the axial compressive load behavior of GFRP-reinforced hollow concrete columns.

Keywords: Design-Oriented, Concrete Modelling, Confinement, GFRP Bars, GFRP Spirals.

INTRODUCTION

Hollow concrete columns (HCCs) are economical and practical for the construction of bridge piers, ground piles, and electric poles because they use fewer materials and significantly reduce weight, leading to a structure with a high strength-to-weight ratio and minimal cost[1-4]. The design and behavior of steel-reinforced HCCs are affected by several parameters such as inner-to-outer diameter ratio (i/o)[2-5], longitudinal-reinforcement ratio (ρ)[4, 6], volumetric ratio (ρ_v)[1, [3, 4, 7], and concrete compressive strength (f_c')[8]. Zhan et al.[5] observed that increasing the *i/o* from 0.53 to 0.73 in steel-reinforced HCCs results in a brittle failure of the concrete core and around 50% reduction in deformation capacity. Lee et al.[4] reported that increasing the reinforcement ratio from 1.17% to 2.00% in HCCs increased the cyclic-load capacity and allowed the specimens to withstand 48% higher lateral loads at the same level of lateral displacement. At the same time, the column ductility decreased by 20% due to the wide and severe crushing of the inner concrete wall. They also observed that reducing the lateral-reinforcement spacing from 80 mm (3.1 in) to 40 mm (1.6 in) increased ductility by 20% and minimized damage in the inner concrete core. On the other hand, Mo et al.[8] found that high-strength concrete (f_c' of 50 MPa (7.3 ksi)) instead of normal-strength concrete (30 MPa (4.4 ksi)) provided stiffer compression resistance in HCC, but with up to a 50% reduction in ductility due to faster crack propagation and easier concrete splitting. These studies showed that these important parameters mainly affect the capacity and deformation of such columns. Relaxing the design of these parameters leads this structure to be more vulnerable to steel corrosion problem due to their high exposed surface area owing to the void existence, which may lead to a dysfunctional structural element. Li et al.[9] and Pantelides et al.[10] found that steel corrosion reduced the axial-load capacity of the concrete columns they tested and negated lateral confinement by damaging the lateral steel reinforcement.

Recently, glass-fiber-reinforced-polymer (GFRP) bar has emerged as an effective alternative to steel as internal reinforcement in concrete structures exposed to severe environmental conditions in order to prevent corrosion problems[11]. Some authors, on the other hand, have reported that GFRP bars are more compatible with concrete than steel due to their similar moduli of elasticity[11, 12]. Several studies have been conducted to understand the behavior of this construction system and to evaluate the effects of different design parameters. Afifi et al.[13] highlighted that increasing the reinforcement ratio from 1.13% to 3.38% by tripling the bar number from 4 to 12 (15.9 mm (0.63 in) GFRP bars) changed the column failure behavior from brittle to ductile and increased the ductility and confinement efficiency by 117% and 30%, respectively. Moreover, Hadi et al.[14] observed a 33% enhancement in ductility with GFRP-reinforced columns when the spacing between spirals was reduced from 60 mm (2.4 in) to 30 mm (1.2 in). These studies motivated investigation of the behavior of HCCs incorporating GFRP reinforcement, as pioneered by AlAjarmeh et al.[15, 16]. This study was the first to explore the potential of GFRP bars and spirals as reinforcing materials for hollow concrete columns to develop a high structural efficiency and corrosion resistant construction system. The results of their investigation revealed that increasing the i/o in HCCs reinforced with GFRP bars and spirals changed the failure behavior from brittle to a progressive failure[15]. Moreover, the enhancement of the confined strength and deformation capacity of the HCCs was proportional to the increase in i/o. They found, on the other hand, that the increase in ρ increases the axial load capacity and, furthermore, longitudinal reinforcements proved the major contribution in lateral confinement[16]. In addition, a comprehensive experimental program has been conducted by testing large-scale GFRP-reinforced concrete columns to investigate the effects of other critical design parameters such as ρ_v and f_c' on the compressive behavior of HCCs and this work is now under review.

Many researchers have developed analytical models to accurately describe the behavior of new structural systems under compression loads. These models were also developed to minimize the number of experiments to determine the effects of the critical design parameters[17]. With respect to the existing analytical models for concrete columns, the lateral-confinement level (either full or partial) is considered the first step in determining the confined strength and the overall stress–strain behavior. The main limitation of the existing models lies with the difficulty in quantifying the amount and level of lateral confinement correlating to the corresponding confined strength. This is especially true when the lateral confinement is in the form of non-uniform stress, such as provided by lateral reinforcement[18, 19]. The existing analytical models separate the contribution of design parameters such as the confinement status (active or passive)[20], full or partial confinement[18], amount of lateral confinement[21, 22], longitudinal reinforcement[17, 21], section geometry[23], and concrete compressive strength[24]. Currently, GFRP-reinforced solid concrete columns are modeled using the available experimental data or with the existing analytical models for steel-reinforced solid concrete columns that have been modified[17, 18, 21]. These models are limited to predicting behavior up to the maximum load[2, 7], with some models related to fully-wrapped hollow unreinforced concrete sections[25-28].

RESEARCH SIGNIFICANCE

There are no analytical models for hollow reinforced-concrete columns with partial lateral confinement, especially incorporating GFRP reinforcement, or that describing their post-peak behavior. In this study, the modeling procedures for GFRP-reinforced solid concrete columns were modified and examined along the lines of Mander's confinement model[23], which is based on the concrete-plasticity theory to predict the confined strength of GFRP-reinforced HCCs. New analytical model is proposed which considers the constituent materials' contribution to accurately describe the overall compressive behavior of GFRP-reinforced HCCs including the strength capacity and the expected failure mode under advanced loading stages, leading to a precise and safe design. The design recommendations herein may support the work of the technical committees engaged in the development of standards and design provisions for GFRP-RC columns.

SUMMARY OF THE EXPERIMENTAL PROGRAM AND RESULTS

A total of 14 circular hollow concrete columns reinforced with GFRP bars and spirals with specimen dimensions of 250 mm (9.8 in) in diameter by 1 m (39.4 in) in height were prepared and tested under concentric compression loading until failure. The columns have different configurations shown in **Fig. 1** to investigate four influential design parameters: inner-to-outer diameter ratio (i/o), longitudinal-reinforcement ratio (ρ), volumetric ratio (ρ_v), and concrete compressive strength (f_c'). The height-to-diameter ratio was similar to that considered by Maranan et al. (32) and Karim et al. (33), which confirmed eliminating global buckling in the columns with the specified ratio. The use of short column specimens were considered to clearly investigate the effects of the design parameters on the pure axial compressive behavior and without the effects of bucking. These columns were all reinforced with high-modulus sand-coated GFRP bars (Grade III)[29] with physical and mechanical properties determined in accordance with the CSA-807[29] and ACI-440.1R-15[30] codes and as reported by Benmokrane et al.[31] as the reinforcement was taken from the same production lot. The mechanical properties of the reinforcements were determined based on the nominal area of the reinforcement, as recommended by CSA-807[29]. An overview of specimen properties and the material characteristics can be found in **Fig. 1** and **Table 1**, respectively. All columns used concrete with 10 mm size aggregates except for column H90-6#5-100-21 which contains 3mm aggregate size as the low-strength concrete used to manufacture this sample was a pre-mix concrete. All columns were tested under monotonic compressive load using a 2000 kN hydraulic cylinder with a loading rate of 1.5 mm/min. A total of six strain gauges were mounted on each column to measure the strain in the longitudinal reinforcement (2 gauges 3 mm in length), spiral reinforcement (2 gauges 3 mm in length), and outer surface of the concrete (2 gauges 20 mm in length). Steel clamps with a 50 mm in width and 10 mm in thickness were attached to the top and bottom of the columns to avoid the stress concentration and the premature failure. The applied load was measured with a 2000 kN load cell and the axial deformation was recorded using a string pot. All data were recorded with the System 5000 data logger. **Figure 2** shows the test setup and instrumentation for the hollow concrete columns. Detailed information and experimental results can be found in AlAjarmeh et al.[15, 16].

Table 2 shows the test results for the 14 concrete columns under concentric compression loading until failure, which used to evaluate the effect of the aforementioned parameters (*i/o*, ρ, ρ_v, and f_c'). This table includes the gross section area (A_g), total core area (A_{core}), peak loads ($P_1\ and\ P_2$), stress at the peak point (f_{ci}), concrete stress alone at the peak point (f_i), number of longitudinal bars ($\#bar$), bar diameter (d_b), and spacing between spirals (S). The first peak load (P_1) is the maximum load resistance by the entire cross-section area when the concrete cover starts to spall, while the second peak load (P_2) is the maximum load resistance provided by the concrete core. The parameter f_{ci} was calculated by dividing P_1 by A_g, while the f_i was calculated by subtracting the contribution of the GFRP bars from P_1 at the peak point and then dividing the magnitude by A_g. The contribution of the GFRP bars was calculated by multiplying the total area of the bars, their elastic modulus, and the strain at the peak point (ε_i). The parameter ρ was calculated from the nominal area of the longitudinal reinforcement by dividing by A_g, while ρ_v was calculated from the volume of one spiral round divided by the concrete-core volume within one spiral pitch, since the diameter of the inner concrete core was measured from the center of the spirals and the height was the spiral pitch. The identification of all the samples starts with the hollow section diameter followed by the number and diameter of the longitudinal reinforcement. Then comes the spacing between lateral reinforcement, followed by the concrete compressive strength. All of these properties are separated by a hyphen.

EXISTING DESIGN MODELS FOR GFRP-REINFORCED CONCRETE COLUMNS

A number of empirical and analytical design-oriented models have been developed to express the stress–strain behavior of confined concrete solid columns[32, 33]. El Fattah and Mohsen[32] highlighted that most of these models involve the use of steel as a lateral confining material with some models developed for FRP-confining systems. In addition, Ozbakkaloglu et al.[33] reviewed 88 models of fully wrapped or encased columns using FRP as a confining material. In contrast, very few studies have been done on partially confined columns using FRP materials[18, 19] and GFRP reinforcement in solid concrete columns[17, 21, 34]. El Fattah and Mohsen[32] suggested that describing the behavior of GFRP-reinforced solid concrete columns as a form of partially confined columns with a non-uniform lateral stress can be investigated by modifying the confinement models for lateral steel reinforcement.

Existing Design Models: Background

Based on using steel reinforcement as confining materials, El Fattah and Mohsen[32] identified three general approaches for modeling confined concrete: the empirical approach based on experimental test results[35, 36], the physical engineering approach based on the confining stress provided by the lateral reinforcement[23, 37], and a combination of the first two approaches but assuming that no lateral steel yields and using compatibility conditions[38, 39]. According to their review, 50%, 10%, and 40% of the proposed models were based on the first, second, and third approaches, respectively. On the other hand, Lokuge et al.[24] classified the stress–strain models into three main categories as Sargin-based[40], Kent and Park-based[41], and Popovics-based[42] to represent the stress–strain curves of concrete columns. These models were constructed with respect to some selected parameters in the stress–strain curves, then calibrated with the experimental test results. Recently, GFRP-reinforced solid concrete columns have been modeled based on the above approaches and categories. For example, Afifi et al.[17] deployed empirical and physical engineering approaches separately by using the modified Mander model[23] as a confinement model, then they used Muguruma[43] model for stress–strain behavior, which is considered as a mix of Popovics-based[42] and Kent and Park-based[41] models. On the other hand, Hales et al.[21] and Sankholkar[44] used the physical-engineering approach with the modified Mander model[23] for confinement due to the lack of experimental data on GFRP-reinforced concrete columns and then applied the Popovics-based model[42] for stress–strain behavior. It can be concluded that the Mander model[23] for confinement is commonly used because it has been verified with large-scale columns[24]. Therefore, the next section describes the development of the prediction model for GFRP-reinforced HCCs according to the modified Mander model[23].

Modified Mander Model for Confinement

The confinement model proposed by Mander et al.[23] was derived from the Willam–Warnke five-parameter failure criterion[45] based on the plasticity theory of concrete. The Mander-model[23] formula was modified to reflect the accurate behavior of columns reinforced with GFRP bars. This modification refers to the confinement criteria provided by GFRP reinforcement, which differs from steel given the diversity in material behavior[17, 21]. Tobbi et al.[34] reported that the Mander model overestimated the confined strength of GFRP-reinforced concrete columns by 30%. Therefore, the modification was adopted by changing the constants $b_0, b_1,$ and b_2 in the plasticity equation—Eqns. (1 to 4)—which are responsible for showing the relation between mean normal and mean shear stresses, as follows:

$$\frac{\tau_{octa}}{f_{co}} = b_0 + b_1 \frac{\sigma_{octa}}{f_{co}} + b_2 \left(\frac{\sigma_{octa}}{f_{co}}\right)^2 \quad (1)$$

$$\tau_{octa} = \frac{1}{3}\left[(\sigma_x - \sigma_y)^2 + (\sigma_y - \sigma_z)^2 + (\sigma_z - \sigma_x)^2\right]^{0.5} \quad (2)$$

$$\sigma_{octa} = \frac{\sigma_x + \sigma_y + \sigma_z}{3} \quad (3)$$

$$f'_{cc} = f_{co}\left(\frac{3(\sqrt{2}+b_1)}{2b_2} + \sqrt{\left(\frac{3(\sqrt{2}+b_1)}{2b_2}\right)^2 - \frac{9b_0}{b_2} - \frac{9\sqrt{2}}{b_2}\frac{f'_l}{f_{co}}} - 2\frac{f'_l}{f_{co}}\right) \quad (4)$$

where, $\sigma_x = f'_{cc}$, $\sigma_y = \sigma_z = f'_l$, f'_{cc} is the confined strength of the column, and f'_l is the effective lateral confinement suggested by Mander [($f'_l = k_e \times f_l$), where k_e is Eq. (16) and f_l is Eq. (14)]. For the experimental results, f'_{cc} was calculated from the second peak axial load

(P_2) after the yield point or after concrete-cover spalling divided by the total core area (A_{core}) (as shown in **Table 2**), which is the area denoted by the diameter between spiral centers. Using the parabolic regression of the experimental mean shear stress (τ_{octa}) vs. mean normal stress (σ_{octa}) curve provided the constant values of $b_2 = -0.2134, b_1 = -0.9234,$ and $b_0 = 0.0849$, as shown in **Fig. 3**. Accordingly, these constants in Eq. (4) yield a new expression for the confinement-strength equation for GFRP-reinforced HCCs, as shown in Eq. (5). In this equation, the predicted confined strength values ($f'_{cc,n1}$) calculated from the new confinement-strength model [Eq. (5)], in addition to the $f'_{cc,n2}$ and $f'_{cc,n3}$ values, were derived from the confined strength models proposed by Afifi et al. [17, 21] and Hales et al.[17, 21]. This approach, however, resulted in a large discrepancy between the predicted values and the experimental results, as tabulated in **Table 3**.

$$f'_{cc,n1} = f_{co}\left(-3.45 + \sqrt{15.48 + 59.61\frac{f'_l}{f_{co}}} - 2\frac{f'_l}{f_{co}}\right) \tag{5}$$

Comparison with Experimental Results

Referring to **Table 3**, the large discrepancy between the experimental and theoretical confined strengths for the GFRP-reinforced HCCs can be explained as follows. Firstly, the analytical models were developed from limited experimental test results for GFRP-reinforced solid concrete columns with partial confinement[17, 21, 46]. Secondly, the compressive behavior of HCCs differs from that of solid concrete columns due to the biaxial-stress distribution within the confined concrete wall of the hollow sections[28, 47]. Accordingly, the final failure of the GFRP-reinforced HCCs was failure of longitudinal GFRP bars and concrete with no failure in the lateral GFRP spirals. In contrast, the failure mode of GFRP-reinforced solid columns are normally due to the failure in lateral reinforcement followed by a total collapse of the sample[13, 48, 49]. Thirdly, the effect of steel longitudinal bars on the behavior of HCCs has not been investigated before, which can merely be attributed to the unchanged strength contribution after yielding. However, the behavior is entirely different with GFRP bars due to their linear elastic response until failure[14, 48, 49]. Karim et al.[46] suggested considering effect of GFRP bars separately from the concrete due to the apparent strength enhancement resulting from adding GFRP bars, particularly those with a high modulus of elasticity. This finding is evidenced by the typical behavior of steel-reinforced concrete columns that showed only one peak strength at the yield point, followed by a descending or softening stress–strain response until failure[32]. Fourthly, the difficulty of identifying the confined-strength point and the corresponding strain value for reinforced-concrete columns due to the irregular post-peak softening responses from the concrete cover spalling. Different perspectives are available to specify this peak, especially with different ascending and descending post-loading behaviors. For example, Afifi et al.[17] took the point to be just after the peak strength with respect to the concrete core area, while Karim et al.[46] took the second peak load in the post-loading stage for the same condition. A new view of capturing the entire stress–strain behavior of GFRP-reinforced HCCs by considering the constitutive behavior of the concrete and GFRP bars is presented next.

DEVELOPMENT OF A NEW DESIGN-ORIENTED MODEL FOR GFRP-REINFORCED HCCS

Theory and Assumptions

A new model is proposed to accurately describe the compressive behavior of GFRP-reinforced HCCs considering the behavior of the GFRP bars and the partially confined concrete. The first assumption in this model is the linear-elastic theory of the GFRP bars[48, 50] to predict the stress contribution of the longitudinal reinforcement until failure. Stress contribution of GFRP bars ($\overline{f_{GFRP}}$) was calculated using the normalized area of the bars with respect to the total area of the column [Eq. (6)].

$$\overline{f_{GFRP}} = f_{GFRP}\frac{A_{GFRP}}{A_g} = (\varepsilon_{GFRP}E_{GFRP})\frac{A_{GFRP}}{A_g} = (\varepsilon_{GFRP}E_{GFRP})\rho_{GFRP} \quad (6)$$

The second important assumption is the perfect bond between the concrete and GFRP reinforcement, as is evident from the experimental results: no splitting between the bars and concrete was observed, and the failure occurred in the concrete and bars at the same time. This assumption takes on that, at any point in the plane, the axial strain in concrete and GFRP bars is the same[46], which made it possible to subtract the stress contribution of GFRP bars from the total behavior of the column and to establish the stress–strain behavior of the concrete alone, as shown in **Fig. 4**. After subtracting the contribution of GFRP bars, the concrete of all the columns showed softening after reaching the peak concrete strength (f_i) and up until final failure. However, f_i expresses the concrete stress with respect to the total area of the section including the reinforcement area. Therefore, f_i need normalising to be $\overline{f_i}$ for accurately measuring the concrete stress as shown in Eq. (7). On the other hand, the overall behavior ended with rupturing in the longitudinal bars and crushing in concrete core, with no failure of the lateral reinforcement. Therefore, the last strain point of the column is related to the maximum compressive strain capacity of the GFRP bars. **Figure 4** depicts the concrete as having a semi-parabolic ascending behavior followed by an almost linear descending behavior. This indicates that the Kent and Park-based model[41] best represents the concrete stress–strain curves.

$$\overline{f_i} = f_i \times \frac{A_g}{A_{gc}} = f_i \times \frac{A_g}{A_g \times (1-\rho)} = \frac{f_i}{(1-\rho)} \tag{7}$$

Model Development

The compressive behavior of the GFRP-reinforced hollow concrete columns, as shown in **Fig. 4**, can be defined with two main points: the point of the peak strength of the concrete (f_i) and the corresponding inflection strain (ε_i), and the point of the concrete strength at failure (f_{cu}) and its corresponding maximum strain (ε_{cu}). The description of these critical points and their identification in developing the prediction model are discussed in the following subsections.

Peak Strength of Concrete (f_i)

The most noticeable observation for all the columns was the peak stress of concrete (f_i) after subtracting the stress contribution of the longitudinal GFRP bars. According to f_i values tabulated in **Table 2,** the normalized values of f_i ($\overline{f_i}$) are close to that of the unconfined concrete strength ($f_{co} = 0.85f_c'$), which f_{co} represents the concrete stress limit before any cracks on the column outer surface. Showing this finding, the average of $\overline{f_i}$ with respect to f_{co} was plotted against the effective lateral-confinement stiffness [f_l''/f_{co}] (which will be discussed later), as given in **Fig. 5**. It can be concluded that the different levels of lateral confinement considered in this study did not significantly affect the strength enhancement of f_{co}. Therefore, it was assumed that the concrete peak strength for the tested columns is equals to f_{co}. This finding is consistent with Roy and Sozen[51], Kent and Park[41], Lam and Teng[22], and Wu et al.[52], as a result of the passive confinement for the partially confined columns as opposed to the fully confined systems. The lateral confinement, however, had a noticeable effect on the inflection-strain point (ε_i) of $\overline{f_i}$ compared to the strain (ε_{co}) related to f_{co}. This is also consistent with the findings of the researchers cited above. The strain ε_{co} can be calculated with Tasdemir's equation [$\varepsilon_{co} = (-0.067{f_{co}}^2 + 29.9f_{co} + 1053)10^{-6}$][53], which deals with different levels of concrete compressive strength.

Inflection Strain (ε_i)

Inflection strain (ε_i) is taken as the level of concrete strain when spalling of the concrete cover occurs in reinforced concrete, which is different from the typical crushing strain of plain concrete (ε_{co}). Therefore, all the variables $\left((i/o), \rho, \rho_v, f_c'\right)$ in the HCC's design matrix were considered to determine their effect on shifting ε_{co} to ε_i. **Figure 6** shows that the strain enhancement of ε_{co} resulting from changing these parameters created four main factors

($\alpha_1, \alpha_2, \alpha_3,$ and α_4), which can be identified by the strain enhancement factor $\left[\frac{(\varepsilon_i - \varepsilon_{co})}{\varepsilon_{co}}\right]$, as given in Eqns. (8-11). These different factors were derived from the relationship of the concrete inflection strain and unconfined strain to that of the column design parameters. Equation (12) is used to predict ε_i by considering the individual effects of the reinforcement ratio (α_1), concrete compressive strength (α_2), volumetric ratio (α_3) and the inner-to-outer diameter ratio (α_4) to the strain of the unconfined concrete ε_{co}. **Figure 7** shows that Eq. (12) can accurately predict the values of $\left[\frac{\varepsilon_i}{\varepsilon_{co}}\right]$ to within $\pm$15%. **Figure 6(b)** references the compressive-strength levels based on the lowest concrete compressive strength of 21.2 MPa.

$$\alpha_1 = 1.73 \times \rho^{1.36} \tag{8}$$

$$\alpha_2 = -0.42 \times \left(\frac{f_c'}{21.2}\right) + 0.91 \tag{9}$$

$$\alpha_3 = 0.1 \times (\rho_v)^2 + 0.15 \times (\rho_v) + 0.01 \tag{10}$$

$$\alpha_4 = -1.27 \times \left({}^{i}\!/_{o}\right) + 0.74 \tag{11}$$

$$\varepsilon_i = \varepsilon_{co} + 3(\alpha_1\alpha_2\alpha_3\alpha_4)(\varepsilon_{co})^4 \times 10^{15} \tag{12}$$

Ultimate Strain (ε_{cu})

The final failure of the HCCs occurred simultaneously in the longitudinal bars and concrete core. The crushing strain of the GFRP bars was therefore used as the basis for identifying the ultimate strain, ε_{cu}. Some studies have determined the compressive strength of high-elastic-modulus GFRP bars $[E_{GFRP} = (60\ to\ 66)\ GPa\ or\ (870\ to\ 957)\ ksi]$ to be approximately 50% to 67% of their ultimate tensile strength[48-50, 54]. These studies also indicated that the GFRP bars behave differently depending on whether they were embedded in concrete or tested alone. Therefore, in another study conducted by the authors[16], the GFRP-bar crushing strain (ε_{cr}) was modeled using a very representative empirical equation based on ρ and the ratio of the total core area to bar area $\left[\frac{A_{core}}{A_{GFRP}}\right]$, as presented in Eq. (13). As a result, the ultimate-strain point (ε_{cu}) was found to be equal to the GFRP-bar crushing strain (ε_{cr}).

$$\varepsilon_{cu} = \varepsilon_{cr} = \frac{12.73 \times \rho \times \frac{A_{core}}{A_{GFRP}}}{E_{GFRP}} \tag{13}$$

It is important to mention that the ε_{cr} values reported in **Table 4** for columns H90-6#5-100-21 and H90-6#5-50-25 were overestimated and underestimated, respectively. This was due to the first column failing prematurely owing to use of small aggregates size that may initiated many microcracks in the concrete core, which reduced the strength and led to easier concrete crushing. On the other hand, the latter specimen recorded a strain 22% greater than the theoretical value due to the 50 mm (1.97 in) spacing between bars. A comprehensive testing program needs to be conducted to determine the crushing strain of GFRP bars with small slenderness ratios.

Strength at Ultimate Strain **(f_{cu})**

Table 2 shows a discrepancy in f_{cu} values due to differences in effective lateral-confinement stiffness $[f_l''/f_{co}]$, which can account for the descending slope between f_{co} and f_{cu}. The effective lateral confining stress (f_l'') [Eq. (20)] was calculated initially by determining the confining stress provided by the lateral reinforcement [Eqns. (14[15, 16] and 15[30])] [**Fig. 8(a)**]. Reduction factors related to the partial lateral confinement (k_e) were considered: the spacing between longitudinal bars (k_o) and the flexural moment of inertia of the bars with respect to the section's total moment of inertia (k_d). k_e is a common factor first suggested by Sheikh and Uzumeri[37] to represent the effect of using discrete lateral reinforcement [Eq. (16)] [**Fig. 8(b)**]. In contrast, k_o is a factor suggested by the authors[16] to refer to the opening between longitudinal bars according to the same criteria of k_e. This factor accounts for the considerable contribution of lateral confinement measured in the longitudinal bars[55], which prevented the lateral expansion of the concrete core [Eq. (17 and 18)] [**Fig. 8(c)**]. k_d is a factor related to the contribution of the load carried by GFRP bars at the last point in a stress–strain curve[16]. In fact, the presence of GFRP longitudinal bars has a significant effect on the compressive behavior of concrete columns. For example, Karim et al.[46] noticed that using ρ of 2.4% for GFRP longitudinal bars increased the axial load capacity by 50%. Moreover, Hadi et al.[14] estimated that the load contribution of GFRP bars in circular concrete columns was one-half that of steel bars due to the former's linear elastic behavior. Therefore, the increased axial-load capacity of concrete columns reinforced with GFRP bars, especially in the post-loading stage after the yield point, means that the bars can affect lateral confinement. This is because the post-loading behavior depends on the strength of the constituent materials, the lateral resistance of the lateral reinforcement, and the resistance provided by the longitudinal bars. The presence of longitudinal bars with stiffness and dilation ratios different from that of the concrete mitigates the full confining engagement by the lateral reinforcement. Therefore, k_d as a reduction factor for the lateral confinement extracted from the GFRP spirals has been proposed. To evaluate this effect, columns with the same volumetric ratio (ρ_v) — including those with different f_c' — were evaluated by plotting the effect of the normalized moment of inertia of the bars (I_{bar}) to that of the concrete core section (I_{core}) versus the normalized f_{cu} with respect to f_{co}, as shown in **Fig. 9** and Eq. 19 (a and b, respectively). Considering the influential factors ($k_e, k_o, and\ k_d$) for partial lateral confinement, the effective lateral confining stress can be calculated with Eq. (20). In Eq. (20), the maximum between k_e and k_o needs to be considered because the higher value will prevent the degradation of the confined concrete core to reach the maximum confined strength. The resulting lateral confinement is then reduced by k_d factor as the linear elastic longitudinal GFRP bars are still acting with concrete in resisting the axial load until failure.

$$f_l = \frac{2A_h K_\varepsilon f_{bent}}{S(D_s - D_i)} \tag{14}$$

$$f_{bent} = (0.05\frac{r}{d_s} + 0.3)f_u \leq f_u \tag{15}$$

$$k_e = \frac{A_{ce}}{A_{cc}} = \frac{\frac{\pi}{4}\left(\left(D_s - \frac{s'}{4}\right)^2 - D_i^2\right)}{\frac{\pi}{4}(D_s^2 - D_i^2)(1-\rho_e)} \tag{16}$$

$$k_o = \frac{A_d}{A_{cc}} = \frac{x{D_s}^2 - D_i^2}{(D_s^2 - D_i^2)(1-\rho_e)} \tag{17}$$

$$x = \left(\frac{1}{2} + \frac{\cos\left(\frac{\theta}{2}\right)}{2} - \left(\frac{\sin\left(\frac{\theta}{2}\right)\tan\left(45 - \frac{\theta}{2}\right)}{4}\right)\right)^2 \tag{18}$$

$$k_d = -\frac{\left[\left(\frac{I_{bars}}{I_{core}}\right)f_{co}\right]^2}{10^7} + 4\frac{\left(\frac{I_{bars}}{I_{core}}\right)f_{co}}{10^5} + 0.59\,; \quad f_{co}\ in\ MPa \tag{19.a}$$

$$k_d = -6\frac{\left[\left(\frac{I_{bars}}{I_{core}}\right)f_{co}\right]^2}{10^6} + 2\frac{\left(\frac{I_{bars}}{I_{core}}\right)f_{co}}{10^4} + 0.59\,; \quad f_{co}\ in\ ksi \tag{19.b}$$

$$f_l'' = Max(k_e, k_o) \times k_d \times f_l \tag{20}$$

The effect of the effective lateral confinement stiffness $[f_l''/f_{co}]$ on the confined strength of concrete at the last point can be seen in Eq. (21) and **Fig. 10**. Consequently, **Table 4** shows a comparison between the experimental and analytical results for the main two points in x and y axes resulted in a good agreement.

$$\frac{f_{cu}}{f_{co}} = 0.175 \times ln\left(\frac{f_l''}{f_{co}}\right) + 1.029 \tag{21}$$

Effect of Concrete-Cover Spalling

Reaching the concrete f_{co} cause a spalling in the concrete cover. At this point, high stress is concentrated at the core by the lateral confinement provided by the GFRP spirals. The effect of concrete cover spalling or the confined stress in the core in the behavior of HCC can be accounted by considering the stresses (unconfined and confined) with respect to their corresponding area as suggested by Pantelides et al.[10] and Hales et al.[21] and by complying Eq. (22). Hereby, confined stress (f_{cc}) can be calculated by Eq. (23). The strain of 0.003 is recommended by ACI 318[56], although, if ε_i is greater, it shall be used instead of 0.003. The value of f_{cc} at this level of strain is considered to be maximum for confined-concrete strength due to the increase in GFRP-bar contribution and the softening behavior of the concrete. Applying Eq. (22) for all tested columns resulted in the second part of the equation to be more dominant as shown in the tabulated results in **Table 5**. This means that the total area of concrete is more realistic to be taken into account instead of the core concrete area.

$$f_{cc} \times A_{cc} \geq f_{co} \times A_{gc} \tag{22}$$

$$f_{cc} = \left(f_{ci} - \frac{\varepsilon_{cc} E_{GFRP} A_{GFRP}}{A_g}\right)\left(\frac{A_{gc}}{A_{cc}}\right); \qquad \varepsilon_{cc} = the\ greater\ of\ (0.003\ or\ \varepsilon_i) \tag{23}$$

Development of the Stress–Strain (f_c $vs.$ ε_c) Relationship

Modeling the stress–strain relationship (f_c vs ε_c) is important in analyzing and designing concrete columns as well as in assessing their strength and deformability. Firstly, the analysis requires that the f_c vs ε_c behavior of each material in the column and their combined effects be identified. Then mathematical formulae must be generalized and developed to describe the entire f_c vs ε_c relationship. In this study, the model was simplified to express the compressive behavior of the nonhomogeneous columns with GFRP reinforcement. The relationship accounted for the main influential factors ($\overline{f_i}, \varepsilon_i, \varepsilon_{cu},$ and f_{cu}) which are a function of number and diameter of longitudinal reinforcement, ratio of inner-to-outer diameter, spacing between transverse reinforcement, and concrete compressive strength, respectively. As seen in **Fig. 4**, the experimental f_c vs ε_c of concrete included two segments, i.e., the ascending (0 to ε_i) and descending (ε_i to ε_{cu}) segments of concrete behavior. In addition, an ascending linear elastic line representing the behavior of GFRP bars started from the beginning up until failure. The summation of these concrete and GFRP responses is the total compressive behavior of the GFRP-reinforced hollow concrete columns.

Ascending Segment of Concrete Behavior

There are many empirical models that can describe the ascending confined and unconfined concrete behavior[22, 57, 58]. Hognestad's ascending parabolic equation[59] is one of the most widely used models, as in the model based on Kent and Park[41]. This parabola is commonly used to describe the ascending part of the stress–strain curve of unconfined concrete based on BS 8110[60] and Eurocode 8[61]. It has also been adopted for FRP-confined concrete[52, 62]. Therefore, referring to the procedures mentioned above [**Fig. 4**] and observations [**Fig. 5**], Hognestad's equation was adopted to develop the model in this study [Eq. (24.a)] but adopting ε_{ci} (calculated using Eq. 12) as a strain value at the peak strength of the column instead of a fixed value of $\varepsilon_{co} = 0.002$ as suggested by Hognestad[59], and the stress contribution of the GFRP bars to concrete was considered based on linear elastic theory as the additional term ($\overline{f_{GFRP}}$) in Eq. (24.a).

$$f_c = f_{co}\left[\left(\frac{2\varepsilon_c}{\varepsilon_i}\right) - \left(\frac{\varepsilon_c}{\varepsilon_i}\right)^2\right] + \overline{f_{GFRP}}; \qquad if\ 0 \le \varepsilon_c \le \varepsilon_i \qquad (24.a)$$

Descending Segment of Concrete Behavior

Simplifying the stress–strain behavior of each component by subtracting the stress contribution of the GFRP bars from the total stress–strain behavior of the column clearly highlighted the softening behavior of the concrete after f_{co} [**Fig. 4**]. All the columns exhibited an almost descending linear line with a negative slope from f_{co} until f_{cu}. This behavior was captured by representing a descending linear line [Eq. (24.b)] between the points (ε_i, f_{co}) and (ε_{cu}, f_{cu}) in the idealized stress-strain curve in **Fig. 6**, where the values of ε_i and f_{cu} are identified in Eqns. 14 and 21. The softening behavior commonly occurs with steel-reinforced[32], GFRP-reinforced[17], and FRP-confined[63] concrete columns with low lateral confinement. This reducing linear post-peak response was previously implemented by Wu et al.[52] and Muguruma[43] for rectangular plain concrete columns with full concrete confinement. The continuous stress contribution of the GFRP bars ($\overline{f_{GFRP}}$) was added until bar failure strain ($\varepsilon_{cu} = \varepsilon_{cr}$).

$$f_c = \left[f_{co} + \left(\frac{(f_{cu}-f_{co})(\varepsilon_c-\varepsilon_i)}{(\varepsilon_{cu}-\varepsilon_i)}\right)\right] + \overline{f_{GFRP}}; \qquad if\ \varepsilon_i < \varepsilon_c \le \varepsilon_{cu} \qquad (24.b)$$

VALIDITY OF THE PROPOSED DESIGN-ORIENTED MODEL

The good agreement between theoretical and experimental (load-strain) test results shown in **Fig. 11** validates that the proposed model can reliably represents the axial compressive-load behavior of the tested GFRP-reinforced hollow concrete columns. The theoretical load–strain behavior in this figure was calculated by multiplying the stress value (f_c) from Eqns. 24 (a and b) by the total cross-sectional area of the hollow column (A_g). The small variation between the predicted and experimental results for column H90-6#5-100-21 [**Fig. 11(l)**, which shows a descending line from the theoretical prediction] was due to the effect of aggregate size (maximum aggregate size was 3 mm instead of 10 mm for others) as was also discussed by Cui and Sheikh[64]. This behavior was not considered in our study; additional work should investigate the aggregate-size effect on the post-loading behavior. Moreover, it is important to mention that column H90-6#5-N/A-25 in **Fig. 11(i)** (without lateral confinement)—representing an unconfined concrete column—used the Hognestad model[59] without any modification.

CONCLUSIONS

This study proposed a new design-oriented model to accurately describe the behavior of circular hollow concrete columns reinforced with GFRP bars and spirals under concentric compressive loading. This model incorporates four influential design parameters: inner-to-outer diameter ratio (i/o), longitudinal-reinforcement ratio (ρ), lateral-reinforcement ratio (ρ_v), and concrete compressive strength (f_c'). Based on the results the study, the following conclusions have been drawn:

1. The behavior of the hollow concrete columns was strongly affected by the inner-to-outer diameter ratio (i/o), longitudinal reinforcement ratio (ρ), volumetric ratio (ρ_v), and concrete compressive strength (f_c'). More ductile failure due to the increase in the biaxial-stress effect can be observed by increasing the i/o, while increased f_c' increased

column brittleness. On the other hand, increasing ρ and ρ_v increased both the strength and deformation capacity of the HCCs due to the increased stiffness and confinement.

2. The existing concrete plasticity model (originally developed for solid columns) proposed by Mander was not applicable for the GFRP-reinforced hollow concrete columns due to the inner void and the presence of linear-elastic longitudinal reinforcement, which contributed to the concrete's confined strength.
3. The overall behavior of the GFRP-reinforced HCCs was a combination of the axial-stress contribution of the GFRP bars and the softening behavior of concrete once the peak strength had been reached.
4. The maximum capacity of the GFRP-reinforced HCCs was defined by the unconfined-concrete strength and the total column gross area. The corresponding strain value at peak strength depends significantly on the inner-to-outer diameter ratio, longitudinal-reinforcement ratio, volumetric ratio, and concrete compressive strength.
5. The softening behavior of concrete up to the failure of the hollow concrete columns was caused by the partial confinement of concrete core provided by the lateral reinforcements and the contribution of the longitudinal bars. The ultimate strain at failure was govern by the crushing strain of the GFRP bars.
6. The behavior of the GFRP-reinforced HCCs can be reliably described by modeling the concrete's behavior until the peak using the Hognestad model and then Wu or Muguruma's concept of descending linear behavior to represent the softening of the reinforced concrete until failure was adopted. The constitutive variables (inflection point, confined strength, and ultimate strain) in those models were modified based on the experimental results from large-scale hollow concrete columns reinforced with GFRP bars. For analysis and design purposes, the load–strain behavior of GFRP-

reinforced HCCs should be based on the total cross-sectional area of the column throughout its loading history.

7. The proposed design-oriented model can accurately predict the concentric compressive behavior of the hollow concrete columns reinforced with GFRP bars and spirals. This model is more preferable for design and analysis engineers due to ease in identifying critical stress and strain points as well as quantifying material contribution (concrete and GFRP bars) separately.

Additional research however is recommended to further calibrate the model to include other ranges of concrete compressive strength and other types of FRP bars. Moreover, the behavior of hollow concrete columns with bigger cross sectional area and higher slenderness ratio should be investigated. This information will be useful to develop a unified design model for hollow concrete columns reinforced with FRP bars.

ACKNOWLEDGMENTS

The authors would like to thank Pultrall Canada and Inconmat V-ROD Australia for providing the GFRP bars and spirals. The assistance of the technical staff at the Centre of Future Materials in the University of Southern Queensland is gratefully acknowledged. The technical support from the Natural Science and Engineering Research Council of Canada (NSERC) Research Chair in Innovative FRP Reinforcement for Sustainable Concrete Infrastructures (University of Sherbrooke, Canada) is appreciated. The first author would like to thank Tafila Technical University (TTU) in Jordan for awarding him the PhD scholarship.

NOTATIONS:

The following symbols are used in this manuscript:

$\alpha_1 =$ Effect of the reinforcement ratio factor (Eq. 2)

$\alpha_2 =$ Effect of the concrete compressive strength factor (Eq. 3)

$\alpha_3 =$ Effect of the volumetric ratio factor (Eq. 4)

$\alpha_4 =$ Effect of the inner-to-outer diameter ratio factor (Eq. 5)

$\theta =$ The angle between two bars

$A_g =$ Total cross-section area (mm^2) (in^2)

$A_{core} =$ Effective core area denoted by the distance between spiral centres (mm^2) (in^2)

$A_{gc} =$ Concrete area in the section (without bars area) (mm^2) (in^2)

$A_{cc} =$ Concrete core area (without bars area) (mm^2) (in^2)

$A_{GFRP} =$ Total area of the GFRP bars (mm^2) (in^2)

$A_h =$ GFRP-spiral cross-sectional area (mm^2) (in^2)

$A_{ce} =$ Area of the concrete core excluding the crushed concrete part due to unconfined concrete between the spirals (mm^2) (in^2)

$A_d =$ Concrete-core area excluding the crushed concrete part due to the opening effect (mm^2) (in^2)

$b_0, b_1, and\ b_2 =$ Constants (Eq. d)

$d_b =$ Bar diameter (mm) (in)

$D_i =$ Diameter of the inner void (mm) (in)

$d_s =$ Spiral diameter (mm) (in)

$D_s =$ Diameter of spirals on-centres (mm) (in)

$\varepsilon_c =$ Concrete strain

$\varepsilon_{cc} =$ Assumed concrete strain at f_{cc}

$\varepsilon_{co} =$ Unconfined concrete strain

$\varepsilon_{cr} =$ Crushing strain of the GFRP bars (Eq. 7)

$\varepsilon_{cu} =$ Ultimate strain (equals to ε_{cu}) (Eq. 7)

$\varepsilon_i =$ Inflection strain (strain at f_{ci} and f_i) (Eq. 6)

$E_{GFRP} =$ Elastic modulus of GFRP bars (MPa) (ksi)

$f_{bent} =$ Tensile strength of bent GFRP bars, ACI-400.1R-15[30] (MPa) (psi) (Eq. 9)

$f_c =$ Stress in the HCC (MPa) (psi) (Eq. 18)

$f_{cc} =$ Maximum confined strength of the concrete (MPa) (psi) (Eq. 16)

$f_c' =$ Concrete compressive strength at the day of testing the HCCs (MPa) (psi)

$f_{cc}' =$ Concrete confined strength at the second peak load (P_2) (MPa) (psi)

$f_{cc,n1}' =$ Theoretical confined strength using modified Mander model using the experimental results of HCCs (MPa) (psi) (Eq. e)

$f_{cc,n2}' =$ Theoretical confined strength using modified Mander model introduced by Afifi et al. (MPa) (psi)

$f_{cc,n3}' =$ Theoretical confined strength using modified Mander model introduced by Hales et al. (MPa) (psi)

$f_{ci} =$ Axial stress of the column at the first axial peak load (P_1) (MPa) (psi)

$f_{co} =$ Unconfined concrete strength ($0.85 f_c'$) (MPa) (psi)

$f_{cu} =$ Concrete strength at the ultimate strain (ε_{cu}) (MPa) (psi) (Eq. 15)

$f_{GFRP} =$ Stress contribution by GFRP bars (MPa) (psi) (Eq. 1)

$f_i =$ Concrete strength alone at the first axial peak load (P_1) (psi) (MPa)

$f_l =$ Lateral confining stress (MPa) (psi) (Eq. 8)

$f_l' =$ Effective lateral confining stress suggested by Mander (MPa) (psi)

$f_l'' =$ Effective lateral confining stress considering the proposed reduction factor in this study (MPa) (psi) (Eq. 14)

$i/o =$ Inner-to-outer diameter ratio

$I_{bar} =$ Moment of inertia of the GFRP bars (mm^4) (in^4)

$I_{core} =$ Moment of inertia of the concrete core (mm^4) (in^4)

$k_d =$ Reduction factor regarding the presence of the GFRP bars in core area (Eq. 12)

$k_e =$ Reduction factor regarding the vertical unconfined area between spirals (Eq. 10)

$k_o =$ Reduction factor regarding the lateral spacing between GFRP bars (Eq. 11)

$K_\varepsilon =$ The proportion of ultimate strain in GFRP spirals before failure to their ultimate tensile strength (0.462 as an average)

$P_1 =$ First axial peak load (kN) (kips)

$P_2 =$ Second axial peak load (kN) (kips)

$\rho =$ Reinforcement ratio with respect to the total cross-section area (A_g)

$\rho_e =$ Effective reinforcement ratio with respect to the effective core area

$\rho_v =$ Volumetric ratio of the lateral reinforcements

$r =$ Inner radius of the spiral (mm) (in)

$\sigma_{octa} =$ Mean normal stress (MPa) (psi) (Eq. c)

$\sigma_x \; and \; \sigma_y =$ Lateral stresses perpendicular to the centre line of the sample (equal f_l) (MPa) (psi)

$\sigma_z =$ Axial stress (MPa) (psi)

$S =$ Vertical spacing of spirals on-centres (mm) (in)

$s' =$ Clear vertical spacing between spirals (mm) (in)

$\tau_{octa} =$ Mean shear stress (MPa) (psi) (Eq. b)

$x =$ Reduction factor for D_s related to the lateral spacing between bars

REFERENCES

1. Lignola GP, Prota A, Manfredi G, Cosenza E, 2007, "Experimental performance of RC hollow columns confined with CFRP," Journal of Composites for Construction, V. 11, No. 1, pp. 42-9.
2. Kusumawardaningsih Y, Hadi MN, 2010, "Comparative behaviour of hollow columns confined with FRP composites," Composite Structures, V. 93, No. 1, pp. 198-205.
3. Hadi M, Le T, 2014, "Behaviour of hollow core square reinforced concrete columns wrapped with CFRP with different fibre orientations," Construction and Building Materials, V. 50, pp. 62-73.
4. Lee J-H, Choi J-H, Hwang D-K, Kwahk I-J, 2015, "Seismic performance of circular hollow RC bridge columns," KSCE Journal of Civil Engineering, V. 19, No. 5, pp. 1456-67.
5. Zahn F, Park R, Priestley M, 1990, "Flexural strength and ductility of circular hollow reinforced concrete columns without confinement on inside face," Structural Journal, V. 87, No. 2, pp. 156-66.
6. Hoshikuma J, Priestley M, 2000, "Flexural behavior of circular hollow columns with a single layer of reinforcement under seismic loading," SSRP, pp. 13.
7. Yazici V, 2012, "Strengthening hollow reinforced concrete columns with fibre reinforced polymers." University of Wollongong.
8. Mo Y, Wong D, Maekawa K, 2003, "Seismic performance of hollow bridge columns," Structural Journal, V. 100, No. 3, pp. 337-48.
9. Li J, Gong J, Wang L, 2009, "Seismic behavior of corrosion-damaged reinforced concrete columns strengthened using combined carbon fiber-reinforced polymer and steel jacket," Construction and Building Materials, V. 23, No. 7, pp. 2653-63.

10. Pantelides CP, Gibbons ME, Reaveley LD, 2013, "Axial load behavior of concrete columns confined with GFRP spirals," Journal of Composites for Construction, V. 17, No. 3, pp. 305-13.

11. Manalo A, Benmokrane B, Park K-T, Lutze D, 2014, "Recent developments on FRP bars as internal reinforcement in concrete structures," Concrete in Australia, V. 40, No. 2, pp. 46-56.

12. Maranan G, Manalo A, Benmokrane B, Karunasena W, Mendis P, Nguyen T, 2018, "Shear behaviour of geopolymer-concrete beams transversely reinforced with continuous rectangular GFRP composite spirals," Composite Structures, V. 187, pp. 454-65.

13. Afifi MZ, Mohamed HM, Benmokrane B, 2013, "Axial capacity of circular concrete columns reinforced with GFRP bars and spirals," Journal of Composites for Construction, V. 18, No. 1.

14. Hadi MN, Karim H, Sheikh MN, 2016, "Experimental investigations on circular concrete columns reinforced with GFRP bars and helices under different loading conditions," Journal of Composites for Construction, V. 20, No. 4.

15. AlAjarmeh OS, Manalo A, Benmokrane B, Karunasena W, Mendis P, Nguyen K, 2019a, "Compressive behavior of axially loaded circular hollow concrete columns reinforced with GFRP bars and spirals," Construction and Building Materials, V. 194, pp. 12-23.

16. AlAjarmeh OS, Manalo AC, Benmokrane B, Karunasena W, Mendis P, 2019b, "Axial performance of hollow concrete columns reinforced with GFRP composite bars with different reinforcement ratios," Composite Structures, V. 213, No. 1, pp. 12.

17. Afifi MZ, Mohamed HM, Benmokrane B, 2015, "Theoretical stress–strain model for circular concrete columns confined by GFRP spirals and hoops," Engineering Structures, V. 102, pp. 202-13.

18. Zeng J-J, Guo Y-C, Gao W-Y, Chen W-P, Li L-J, 2018, "Stress-Strain Behavior of Circular Concrete Columns Partially Wrapped with FRP Strips," Composite Structures.

19. Zeng J-J, Guo Y-C, Gao W-Y, Li J-Z, Xie J-H, 2017, "Behavior of partially and fully FRP-confined circularized square columns under axial compression," Construction and Building Materials, V. 152, pp. 319-32.

20. Candappa D, Sanjayan J, Setunge S, 2001, "Complete triaxial stress-strain curves of high-strength concrete," Journal of Materials in Civil Engineering, V. 13, No. 3, pp. 209-15.

21. Hales TA, Pantelides CP, Sankholkar P, Reaveley LD, 2017, "Analysis-oriented stress-strain model for concrete confined with fiber-reinforced polymer spirals," ACI Structural Journal, V. 114, No. 5, pp. 1263.

22. Lam L, Teng J, 2003, "Design-oriented stress–strain model for FRP-confined concrete," Construction and building materials, V. 17, No. 6-7, pp. 471-89.

23. Mander JB, Priestley MJ, Park R, 1988, "Theoretical stress-strain model for confined concrete," Journal of structural engineering, V. 114, No. 8, pp. 1804-26.

24. Lokuge WP, Sanjayan J, Setunge S, 2005, "Stress–strain model for laterally confined concrete," Journal of Materials in Civil Engineering, V. 17, No. 6, pp. 607-16.

25. Lignola GP, Prota A, Manfredi G, Cosenza E, 2008, "Unified theory for confinement of RC solid and hollow circular columns," Composites Part B: Engineering, V. 39, No. 7, pp. 1151-60.

26. Cascardi A, Micelli F, Aiello MA, 2016, "Unified model for hollow columns externally confined by FRP," Engineering Structures, V. 111, pp. 119-30.

27. Fam AZ, Rizkalla SH, 2001, "Confinement model for axially loaded concrete confined by circular fiber-reinforced polymer tubes," Structural Journal, V. 98, No. 4, pp. 451-61.

28. Yazici V, Hadi MN, 2012, "Normalized confinement stiffness approach for modeling FRP-confined concrete," Journal of composites for construction, V. 16, No. 5, pp. 520-8.

29. CSA, 2012, "Design and construction of building structures with fibre-reinforced polymers." Canadian Standards Association, CAN/CSA-S806-12, Rexdale, ON, Canada.

30. ACI, 2015, "Guide for the Design and Construction of Concrete Reinforcedwith FRP Bars (440.1R-15)," American Concrete Institute, Farmington Hills, MI.

31. Benmokrane B, Manalo A, Bouhet J-C, Mohamed K, Robert M, 2017, "Effects of Diameter on the Durability of Glass Fiber–Reinforced Polymer Bars Conditioned in Alkaline Solution," Journal of Composites for Construction, V. 21, No. 5, pp. 04017040.

32. Abd El Fattah AM, 2012, "Behavior of concrete columns under various confinement effects." Kansas State University.

33. Ozbakkaloglu T, Lim JC, Vincent T, 2013, "FRP-confined concrete in circular sections: Review and assessment of stress–strain models," Engineering Structures, V. 49, pp. 1068-88.

34. Tobbi H, Farghaly AS, Benmokrane B, 2014, "Strength model for concrete columns reinforced with fiber-reinforced polymer bars and ties," ACI Structural Journal, V. 111, No. 4, pp. 789-98.

35. Fafitis A, Shah S, 1985, "Lateral reinforcement for high-strength concrete columns," ACI Special Publication, V. 87, pp. 213-32.

36. Hoshikuma J, Kawashima K, Nagaya K, Taylor A, 1997, "Stress-strain model for confined reinforced concrete in bridge piers," Journal of Structural Engineering, V. 123, No. 5, pp. 624-33.

37. Sheikh SA, Uzumeri SM, 1980, "Strength and ductility of tied concrete columns," Journal of the structural division, V. 106, No. ASCE 15388 Proceeding.

38. Cusson D, Paultre P, 1995, "Stress-strain model for confined high-strength concrete," Journal of Structural Engineering, V. 121, No. 3, pp. 468-77.

39. Saatcioglu M, Razvi SR, 1992, "Strength and ductility of confined concrete," Journal of Structural engineering, V. 118, No. 6, pp. 1590-607.

40. Sargin M, 1971, "Stress-Strain relationships for concrete and analysis of structural concrete sections," Study No 4, Solid Mechanics Division, University of Waterloo, Waterloo, Ontario, Canada.

41. Kent DC, Park R, 1971, "Flexural members with confined concrete," Journal of the Structural Division, V. 97, No. 7, pp. 1969-90.

42. Popovics S, 1973, "A numerical approach to the complete stress-strain curve of concrete," Cement and concrete research, V. 3, No. 5, pp. 583-99.

43. Muguruma H, 1980, "A stress-strain model of confined concrete," Annual Report on Cement Engineering, V. 34, pp. 429-32.

44. Sankholkar PP, 2016, "Confinement model for concrete columns internally reinforced with glass fiber reinforced polymer spirals." The University of Utah.

45. Willam KJ, 1975, "Constitutive model for the triaxial behaviour of concrete," Proc Intl Assoc Bridge Structl Engrs, V. 19, pp. 1-30.

46. Karim H, Sheikh MN, Hadi MN, 2016, "Axial load-axial deformation behaviour of circular concrete columns reinforced with GFRP bars and helices," Construction and Building Materials, V. 112, pp. 1147-57.

47. Yazici V, Hadi MN, 2009, "Axial load-bending moment diagrams of carbon FRP wrapped hollow core reinforced concrete columns," Journal of Composites for Construction, V. 13, No. 4, pp. 262-8.

48. Tobbi H, Farghaly AS, Benmokrane B, 2014, "Behavior of concentrically loaded fiber-reinforced polymer reinforced concrete columns with varying reinforcement types and ratios," ACI Structural Journal, V. 111, No. 2, pp. 375.

49. Maranan G, Manalo A, Benmokrane B, Karunasena W, Mendis P, 2016, "Behavior of concentrically loaded geopolymer-concrete circular columns reinforced longitudinally and transversely with GFRP bars," Engineering Structures, V. 117, pp. 422-36.

50. Deitz D, Harik I, Gesund H, 2003, "Physical properties of glass fiber reinforced polymer rebars in compression," Journal of Composites for Construction, V. 7, No. 4, pp. 363-6.

51. Roy H, Sozen MA, 1965, "Ductility of concrete," Special Publication, V. 12, pp. 213-35.

52. Wu G, Wu Z, Lü Z, 2007, "Design-oriented stress–strain model for concrete prisms confined with FRP composites," Construction and Building Materials, V. 21, No. 5, pp. 1107-21.

53. Tasdemir M, Tasdemir C, Akyüz S, Jefferson A, Lydon F, Barr B, 1998, "Evaluation of strains at peak stresses in concrete: a three-phase composite model approach," Cement and Concrete Composites, V. 20, No. 4, pp. 301-18.

54. Fillmore B, Sadeghian P, 2018, "Contribution of Longitudinal GFRP Bars in Concrete Cylinders under Axial Compression," Canadian Journal of Civil Engineering, V. 45, No. 6, pp. 458-68.

55. Karim H, Noel-Gough B, Sheikh MN, Hadi MN, 2015, "Strength and ductility behavior of circular concrete columns reinforced with GFRP bars and helices."

56. ACI, 2008, "(American Concrete Institute), Building Code Requirements for Structural Concrete.," ACI 318-08 and Commentary, Farmington Hills, MI, pp. 471.

57. Yang K-H, Mun J-H, Cho M-S, Kang TH, 2014, "Stress-strain model for various unconfined concretes in compression," ACI Structural Journal, V. 111, No. 4, pp. 819.

58. Li B, Park R, Tanaka H, 2001, "Stress-strain behavior of high-strength concrete confined by ultra-high-and normal-strength transverse reinforcements," ACI Structural Journal, V. 98, No. 3.

59. Hognestad E, 1951, "Study of combined bending and axial load in reinforced concrete members." University of Illinois at Urbana Champaign, College of Engineering. Engineering Experiment Station.

60. BS B, 1997, "Structural Use of Concrete, Part 1: Code of Practice for Design and Construction," British Standards Institution, UK.

61. Eurocode-8, 2005, "Design of structures for earthquake resistance-part 1: general rules, seismic actions and rules for buildings," Brussels: European Committee for Standardization.

62. Miyauchi K, Inoue S, Kuroda T, Kobayashi A, 2000, "Strengthening effects of concrete column with carbon fiber sheet," Transactions of the Japan Concrete Institute, V. 21, pp. 143-50.

63. Teng J, Jiang T, Lam L, Luo Y, 2009, "Refinement of a design-oriented stress–strain model for FRP-confined concrete," Journal of Composites for Construction, V. 13, No. 4, pp. 269-78.

64. Cui C, Sheikh S, 2010, "Experimental Study of Normal-and High-Strength Concrete Confined with Fiber-Reinforced Polymers," Journal of Composites for Construction, V. 14, No. 5.

LIST OF TABLES AND FIGURES

List of Tables

List of Figures

Table 1. Physical and mechanical properties of the GFRP reinforcement materials[31]

	Properties	Test Method	Tested Samples	Values			
				No. 6	No. 5	No. 4	No. 3
Physical	Nominal bar diameter, mm (in)	CSA S807[29]	9	19.1 (0.79)	15.9 (0.63)	12.7 (0.50)	9.5 (0.37)
Physical	Nominal bar area, mm^2 (in^2)	CSA S807[29]	9	286.5 (0.44)	198.5 (0.31)	126.6 (0.20)	70.8 (0.11)
Physical	Cross-sectional area, mm^2 (in^2)	CSA S807[29]	9	317.3 (0.49)	224.4 (0.35)	145.0 (0.22)	83.8 (0.13)
Mechanical	Tensile strength, f_u, MPa (ksi)	ASTM D7205[30]	6	1270 (184.2) (31.4 (4.5))*	1237 (179.4) (33.3 (4.8))*	1281 (185.8) (35.3 (5.1))*	1315 (190.7) (31.1 (4.5))*
Mechanical	Elastic modulus, E_{GFRP}, GPa (ksi)	ASTM D7205[30]	6	60.5 (877.5) (0.5 (73))*	60.5 (877.5) (1.3 (189))*	61.3 (889.1) (0.4 (58))*	62.5 (906.5) (0.4 (58))*
Mechanical	Ultimate tensile strain, ε_u,%	ASTM D7205[30]	6	2.1 (0.1)*	2.1 (0.1)*	2.1 (0.1)*	2.3 (0.1)*

* Standard division

Table 2. Specimen details, test matrix, and experimental test results

Column	A_g (mm²) (in²)	A_{core} (mm²) (in²)	P_1 (kN) (kips)	P_2 (kN) (kips)	f_{ci} (MPa) (psi)	ε_i $\mu\varepsilon$	f_i (MPa) (psi)	f'_c (MPa) (psi)	# of bars	d_b (mm) (in)	S (mm) (in)	i/o	ρ (%)	ρ_v (%)
H40-6#5-100-32	47807 (74.1)	27083 (42.0)	1408 (317)	1295 (291)	29.4 (4264)	2780	25.2 (3655)	31.8 (4612)	6	15.9 (0.63)	100 (3.94)	0.16	2.49	1.56
H65-6#5-100-32	45746 (70.9)	25022 (38.8)	1559 (350)	1458 (328)	34.1 (4946)	2550	29.9 (4337)	31.8 (4612)	6	15.9 (0.63)	100 (3.94)	0.26	2.60	1.69
H90-6#5-100-32	42704 (66.2)	21980 (34.1)	1411 (317)	1226 (276)	33.0 (4786)	2320	28.8 (4177)	31.8 (4612)	6	15.9 (0.63)	100 (3.94)	0.36	2.79	1.92
H90-6#4-100-25	42704 (66.2)	21980 (34.1)	1035 (233)	985 (221)	24.2 (3510)	2850	21.9 (3176)	25.0 (3626)	6	12.7 (0.50)	100 (3.94)	0.36	1.78	1.92
H90-6#6-100-25	42704 (66.2)	21980 (34.1)	1140 (256)	1248 (281)	26.7 (3873)	2100	19.6 (2843)	25.0 (3626)	6	19.1 (0.75)	100 (3.94)	0.36	4.00	1.92
H90-4#5-100-25	42704 (66.2)	21980 (34.1)	983 (221)	876 (197)	23.0 (3336)	3200	19.0 (2756)	25.0 (3626)	4	15.9 (0.63)	100 (3.94)	0.36	1.86	1.92
H90-8#5-100-25	42704 (66.2)	21980 (34.1)	1268 (285)	1406 (316)	29.7 (4308)	2219	22.8 (3307)	25.0 (3626)	8	15.9 (0.63)	100 (3.94)	0.36	3.72	1.92
H90-9#4-100-25	42704 (66.2)	21980 (34.1)	1035 (233)	1204 (271)	24.2 (3510)	2500	19.8 (2872)	25.0 (3626)	9	12.7 (0.50)	100 (3.94)	0.36	2.67	1.92
H90-6#5-N/A-25	42704 (66.2)	21980 (34.1)	1022 (230)	- (-)	23.9 (3466)	1658	22.3 (3234)	25.0 (3626)	6	15.9 (0.63)	- (-)	0.36	2.79	0.00
H90-6#5-150-25	42704 (66.2)	21980 (34.1)	1108 (249)	1110 (250)	25.9 (3756)	2350	20.5 (2973)	25.0 (3626)	6	15.9 (0.63)	150 (5.91)	0.36	2.79	1.28
H90-6#5-50-25	42704 (66.2)	21980 (34.1)	1197 (269)	1434 (322)	28.0 (4061)	3800	21.9 (3176)	25.0 (3626)	6	15.9 (0.63)	50 (1.97)	0.36	2.79	3.84
H90-6#5-100-21	42704 (66.2)	21980 (34.1)	907 (204)	849 (191)	21.2 (3075)	2350	18.0 (2611)	21.2 (3075)	6	15.9 (0.63)	100 (3.94)	0.36	2.79	2.14

H90-6#5-100-37	42704 (66.2)	21980 (34.1)	1570 (353)	1424 (320)	36.9 (5352)	2203	33.8 (4902)	36.8 (5337)	6	15.9 (0.63)	100 (3.94)	0.36	2.79	2.14
H90-6#5-100-44	42704 (66.2)	21980 (34.1)	1880 (423)	1644 (370)	43.8 (6353)	2181	41.6 (6034)	44.0 (6382)	6	15.9 (0.63)	100 (3.94)	0.36	2.79	2.14

Table 3. Comparison between experimental and theoretical values for f'_{cc}

Column	Experimental results	Eq. (e)		Afifi et al.[17]		Hales et al.[21]	
	f'_{cc} (MPa) (psi)	$f'_{cc,n1}$ (MPa) (psi)	Variation (%)	$f'_{cc,n2}$ (MPa) (psi)	Variation (%)	$f'_{cc,n3}$ (MPa) (psi)	Variation (%)
H40-6#5-100-32	47.8 (6933)	31.3 (4540)	34.5	43.4 (6295)	9.2	36.1 (5236)	24.5
H65-6#5-100-32	58.3 (8456)	34.0 (4931)	41.7	44.1 (6396)	24.4	37.4 (5424)	35.8
H90-6#5-100-32	59.6 (8644)	37.4 (5424)	37.2	44.8 (6498)	24.8	39.2 (5685)	34.2
H90-6#4-100-25	44.8 (6498)	33.1 (4801)	26.1	35.8 (5192)	20.1	32.7 (4743)	27.0
H90-6#6-100-25	56.8 (8238)	34.0 (4931)	40.1	35.8 (5192)	37.0	33.2 (4815)	41.5
H90-4#5-100-25	39.8 (5773)	33.2 (4815)	16.6	35.8 (5192)	10.1	32.8 (4757)	17.6
H90-8#5-100-25	64.0 (9282)	33.9 (4917)	47.0	35.8 (5192)	44.1	33.1 (4801)	48.3
H90-9#4-100-25	.548 (7948)	33.5 (4859)	38.9	35.8 (5192)	34.7	32.9 (4772)	40.0
H90-6#5-150-25	50.5 (7324)	24.9 (3611)	50.7	36.2 (5250)	28.3	29.6 (4293)	41.4
H90-6#5-50-25	65.2 (9456)	56.0 (8122)	14.1	37.9 (5497)	41.9	45.7 (6628)	29.9
H90-6#5-100-21	38.6	31.1	19.4	30.6	20.7	29.3	24.1

	(5598)	(4511)		(4438)		(4250)	
H90-6#5-100-37	64.7 (9384)	40.1 (5816)	38.0	51.2 (7426)	20.9	43.7 (6338)	32.5
H90-6#5-100-44	74.8 (10849)	43.7 (6338)	41.6	60.2 (8731)	19.5	50.1 (7266)	33.0

Table 4. Comparison between experimental values and theoretical results using the proposed model

Column	f_{ci} (MPa) (psi)			$\mu\varepsilon_i$			$\mu\varepsilon_{co}$	f_{cu} (MPa) (psi)			$\mu\varepsilon_{cu}$		
	Exp.	**Theo.**	**(% Dif.)**	**Exp.**	**Theo.**	**(% Dif.)**		**Exp.**	**Theo.**	**(% Dif.)**	**Exp.**	**Theo.**	**(% Dif.)**
H40-6#5-100-32	29.4 (4264)	30.9 (4482)	-5	2780	2611	6	1811	12.8 (1856)	12.0 (1740)	6	10972	12019	-9
H65-6#5-100-32	34.1 (4946)	31.0 (4496)	9	2550	2549	0	1811	13.9 (2016)	12.9 (1871)	7	11109	11605	-4
H90-6#5-100-32	33.0 (4786)	31.6 (4583)	4	2320	2462	-6	1811	14.1 (2045)	13.9 (2016)	1	10620	10920	-3
H90-6#4-100-25	24.2 (3510)	24.8 (3597)	-2	2850	3313	-15	1658	12.8 (1865)	12.2 (1769)	5	10845	10689	1
H90-6#6-100-25	26.7 (3873)	26.6 (3858)	0	2100	2207	-5	1658	11.2 (1624)	11.4 (1653)	-2	10850	10849	0
H90-4#5-100-25	23.0 (3336)	24.8 (3597)	-8	3200	3224	-1	1658	11.9 (1726)	11.9 (1726)	0	11201	10920	3
H90-8#5-100-25	29.7 (4308)	26.8 (3887)	10	2219	2269	-2	1658	10.8 (1566)	12.3 (1784)	-9	11210	10920	3
H90-9#4-100-25	24.2 (3510)	25.4 (3684)	-5	2500	2613	-5	1658	12.4 (1798)	12.6 (1827)	-1	10740	10689	0
H90-6#5-N/A-25	23.9 (3466)	24.1 (3495)	-1	1658	1649	1	1658	- (-)	- (-)	-	4287	-	-
H90-6#5-150-25	25.9 (3756)	25.0 (3626)	3	2350	2250	4	1658	9.6 (1392)	11.1 (1610)	-9	10592	10920	-3
H90-6#5-50-25	28.0 (4061)	28.4 (4119)	-1	3800	3366	11	1658	15.5 (2248)	16.0 (2320)	-3	13284	10920	22
H90-6#5-100-21	21.2 (3075)	22.4 (3249)	-6	2350	2628	-12	1570	4.9 (711)	10.8 (1566)	-120	8301	10920	-24
H90-6#5-100-37	36.9 (5352)	35.2 (5105)	5	2203	2343	-6	1923	16.4 (2379)	15.3 (2219)	6	12756	10920	15
H90-6#5-100-44	43.8 (6353)	41.1 (5961)	6	2181	2204	-1	2078	18.3 (2654)	16.7 (2422)	9	10714	10920	-2

Table 5. Confined strength values (f_{cc}) and the load contribution of the concrete

f_{ci} (MPa) (psi)	$\mu\varepsilon_i$	f_{co} (MPa) (psi)	f_{cc} (MPa) (psi)	f_{cc}/f_{co}	$f_{co} \times A_{gc}$ (kN) (kips)	$f_{cc} \times A_{ce}$ (kN) (kips)
29.4 (4264)	2780	26.5 (3844)	42.9 (6222)	1.62	1236 (278)	1110 (250)
34.1 (4946)	2550	26.5 (3844)	52.4 (7600)	1.97	1182 (266)	1248 (281)
33.0 (4786)	2320	26.5 (3844)	52.8 (7658)	1.99	1101 (248)	1099 (247)
24.2 (3510)	2850	21.3 (3089)	39.9 (5787)	1.88	891 (200)	847 (190)
26.7 (3873)	2100	21.3 (3089)	36.2 (5250)	1.70	871 (196)	733 (165)
23.0 (3336)	3200	21.3 (3089)	37.0 (5366)	1.74	891 (200)	785 (176)
29.7 (4308)	2219	21.3 (3089)	43.0 (6237)	2.03	874 (196)	878 (197)
24.2 (3510)	2500	21.3 (3089)	36.5 (5294)	1.72	883 (199)	760 (171)
23.9 (3466)	1658	22.8 (3307)	- (-)	-	- (-)	- (-)

25.9 (3756)	2350	22.8 (3307)	39.4 (5714)	1.73	946 (213)	820 (184)
28.0 (4061)	3800	22.8 (3307)	40.9 (5932)	1.79	946 (213)	850 (191)
21.2 (3075)	2350	18.0 (2611)	30.6 (4438)	1.70	748 (168)	635 (143)
36.9 (5352)	2203	31.3 (4511)	60.2 (8731)	1.92	1299 (292)	1252 (281)
43.8 (6353)	2181	37.4 (5424)	73.2 (10617)	1.96	1553 (349)	1523 (342)

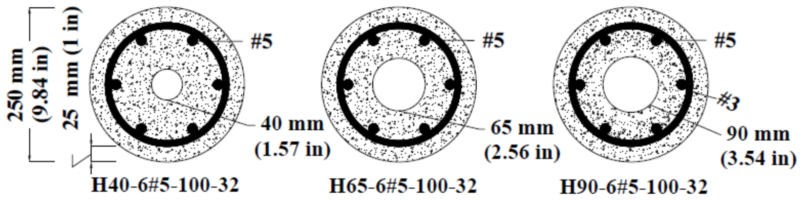

(a) Columns with different Inner-to-outer diameter (i/o) ratio

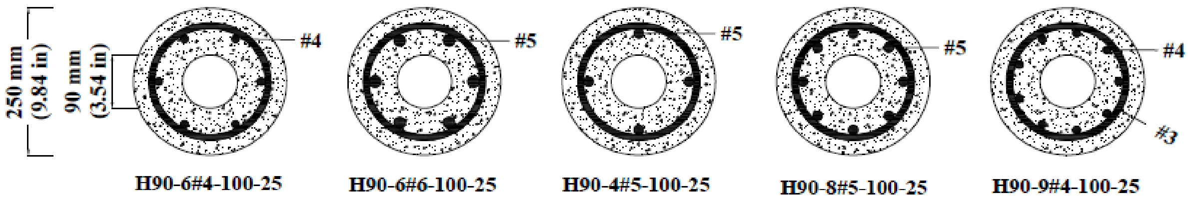

(b) Columns with different reinforcement ratio (ρ)

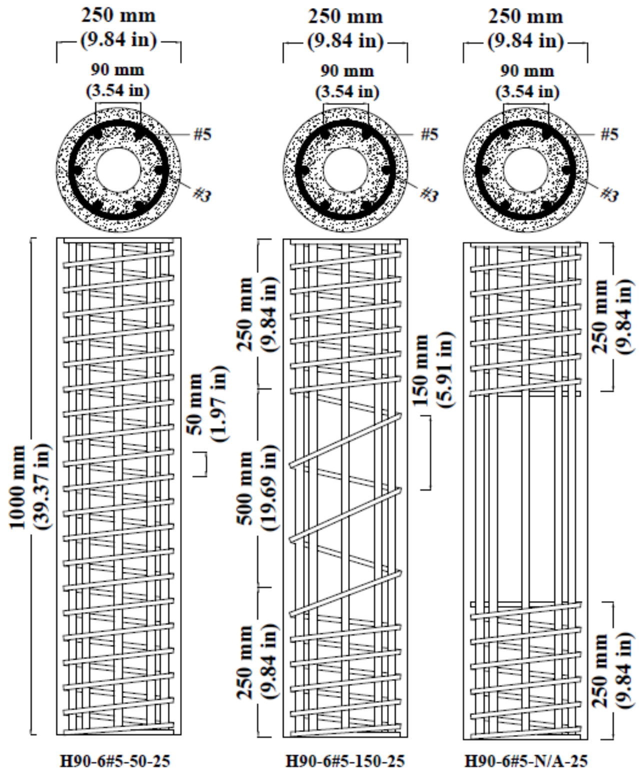

(c) Columns with different volumetric ratio (ρ_v)

Figure 1. Details of the tested GFRP-reinforced hollow concrete columns

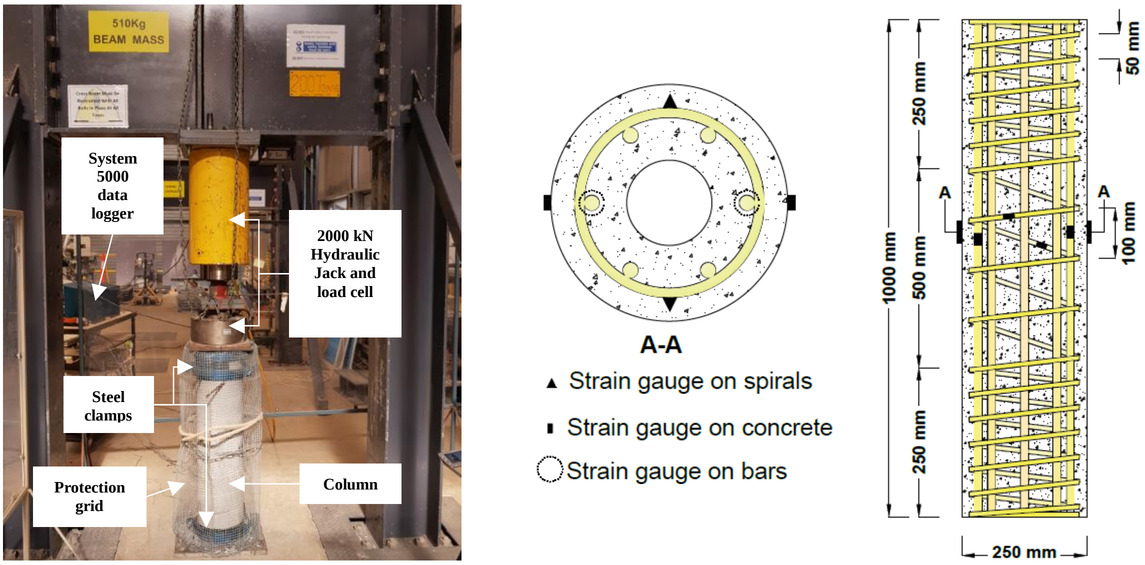

(a) Test setup

(b) Location of strain gauges

Figure 2. Test setup and instrumentation for the GFRP-reinforced hollow concrete columns

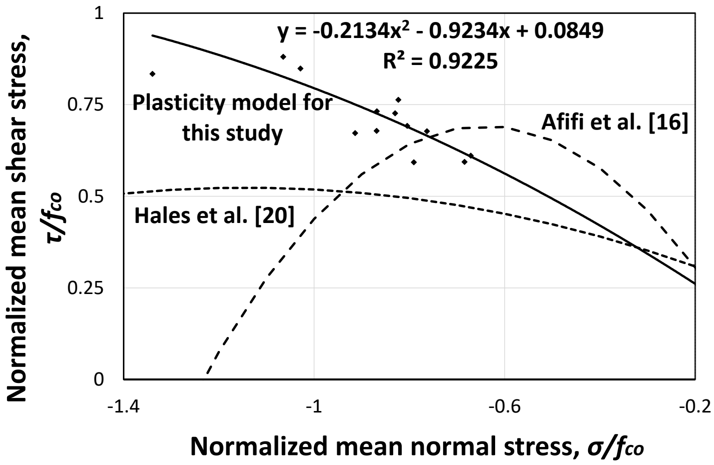

Figure 3. Plasticity model of the experimental results of this study compared with other plasticity models

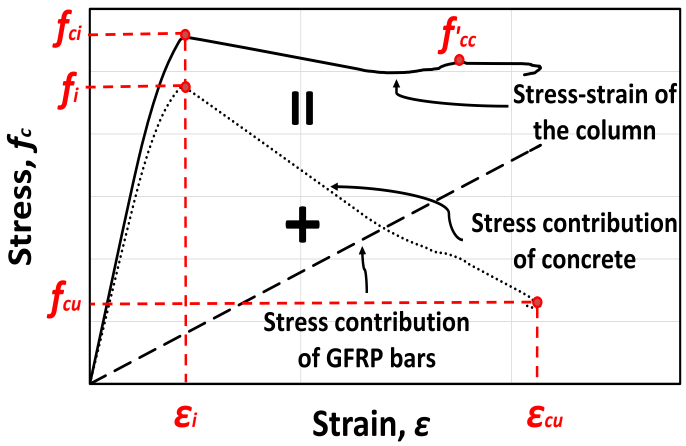

Figure 4. Stress-strain contribution of the column’s components

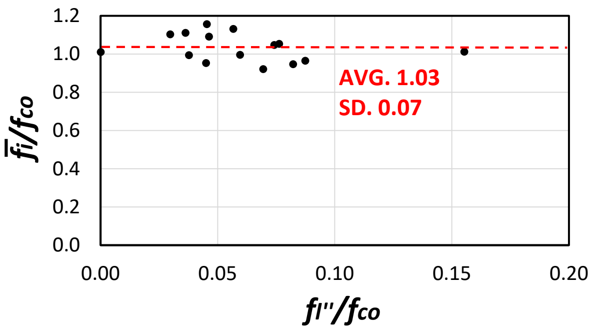

Figure 5. Effect of the effective lateral confinement stiffness on normalised $\overline{f_i}$ over f_{co}

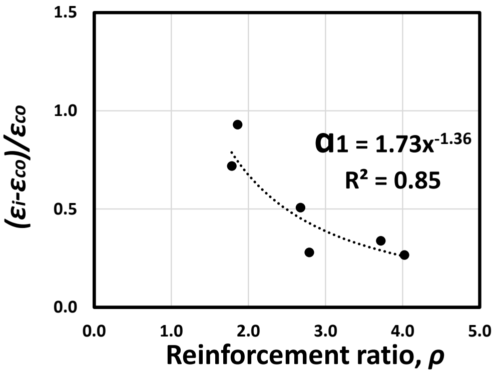

(a) Effect of reinforcement ratio, ρ

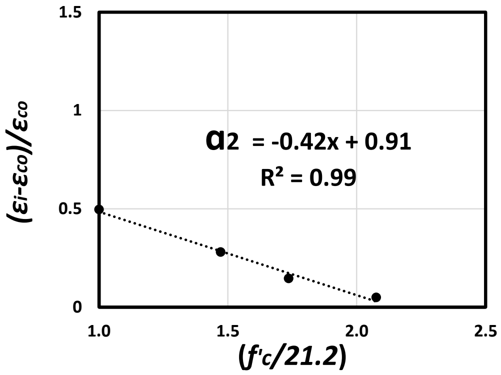

(b) Effect of concrete compressive strength, f_c'

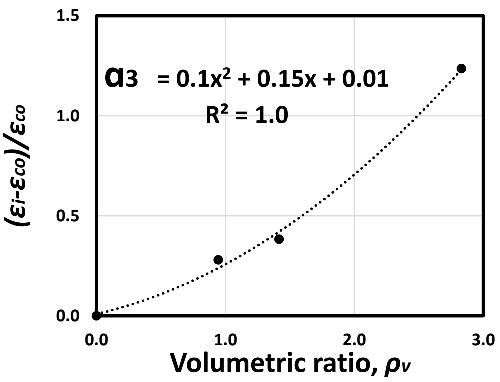

(c) Effect of volumetric ratio, ρ_v

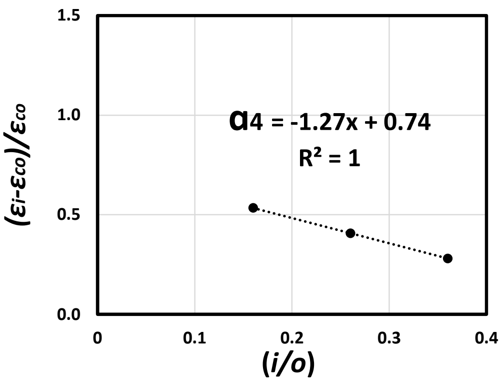

(d) Effect of inner-to-outer diameter (i/o) ratio

Figure 6. The main four factors affecting the inflection strain ε_i

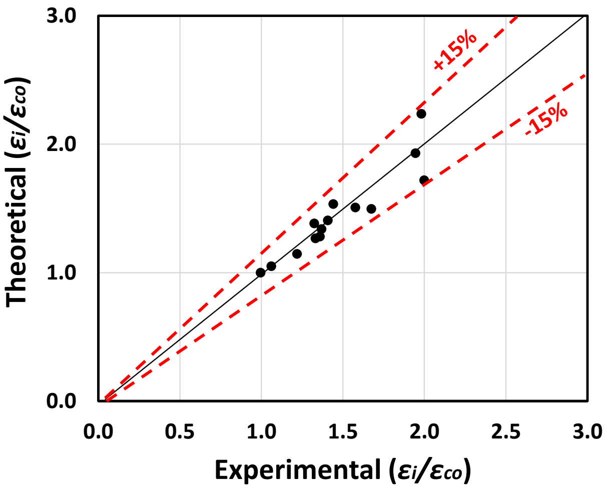

Figure 7. Comparison between Experimental and theoretical normalised inflection strain point $\left[\frac{\varepsilon_i}{\varepsilon_{co}}\right]$

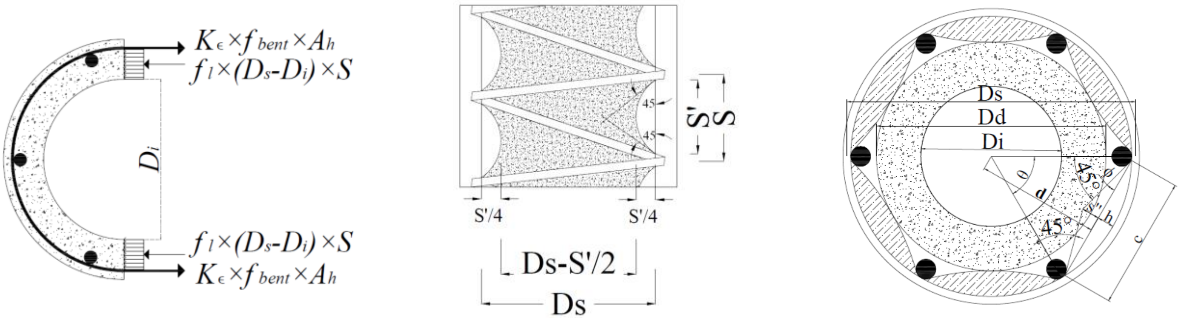

a. Lateral confinement **b.** Vertical spacing effect **c.** Opening effect

Figure 8. Lateral confinement mechanism and confinement efficiency factors

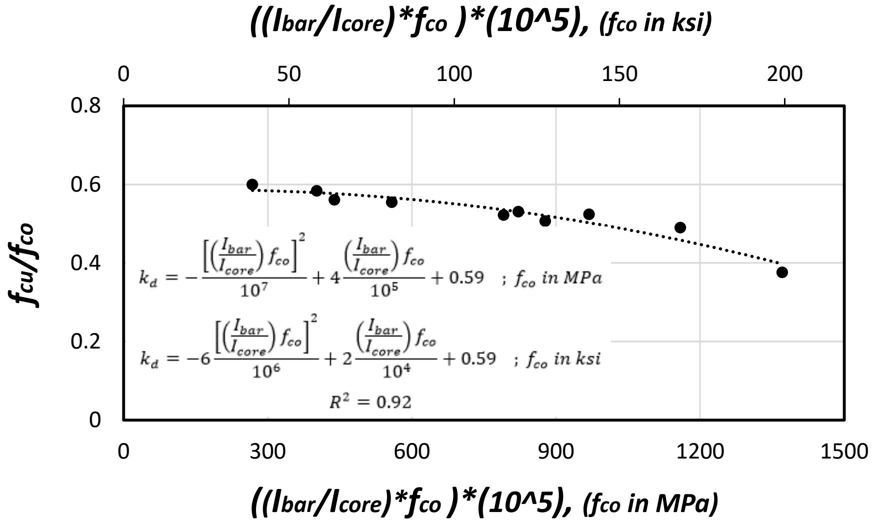

Figure 9. Effect of the longitudinal reinforcement (k_d) in post loading stage

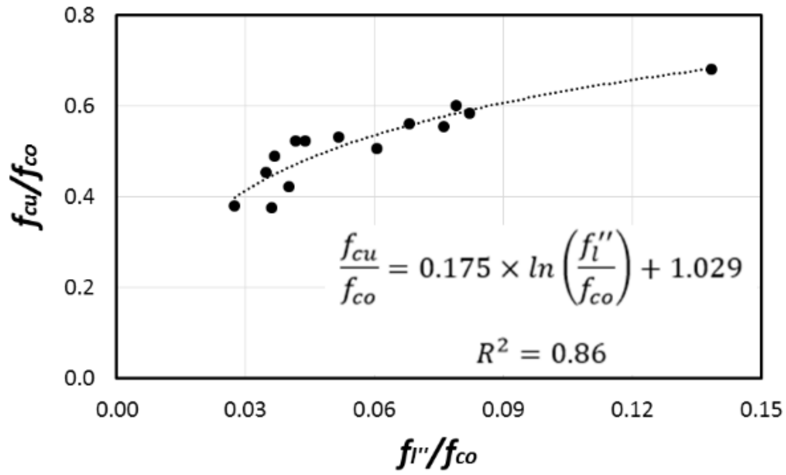

Figure 10. Normalised concrete strength versus lateral confinement stiffness

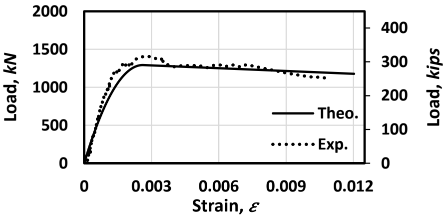

(a) H40-6#5-100-32

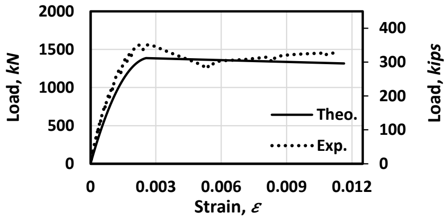

(b) H65-6#5-100-32

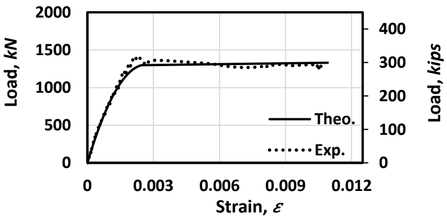

(c) H90-6#5-100-32

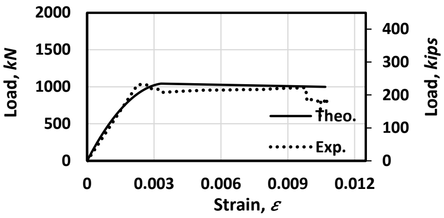

(d) H90-6#4-100-25

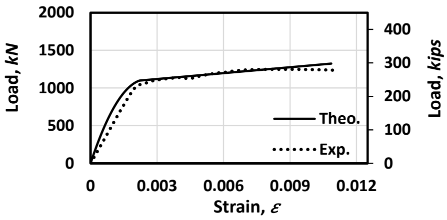

(e) H90-6#6-100-25

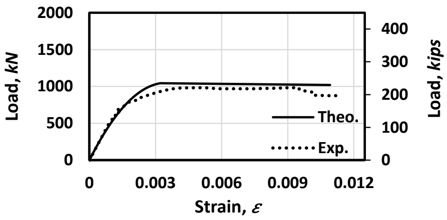

(f) H90-4#5-100-25

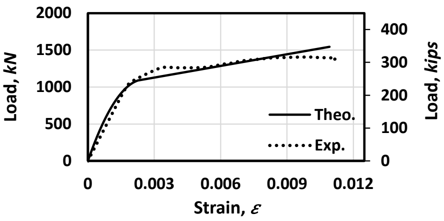

(j) H90-8#5-100-25

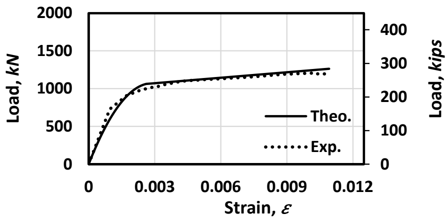

(h) H90-9#4-100-25

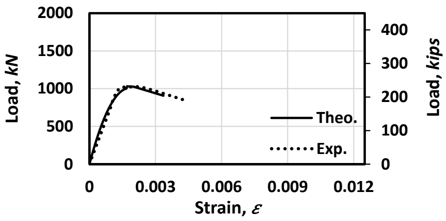

(i) H90-6#5-N/A-25

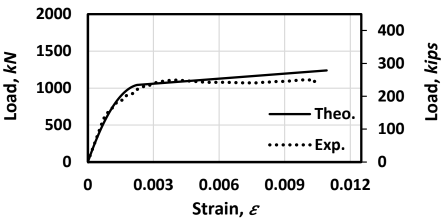

(j) H90-6#5-150-25

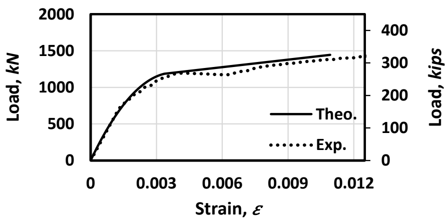

(k) H90-6#5-50-25

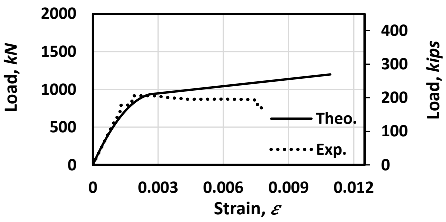

(l) H90-6#5-100-21

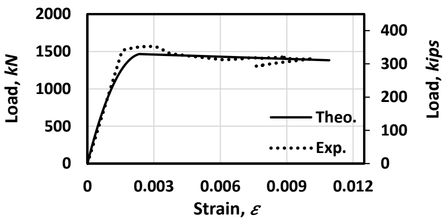

(m) H90-6#5-100-37

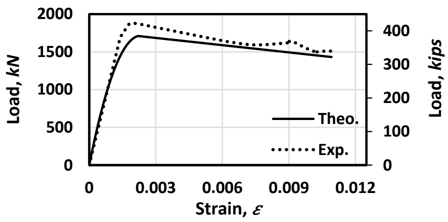

(n) H90-6#5-100-44

Figure 11. Comparison between experimental and proposed stress-strain curves of the GFRP-reinforced hollow concrete columns

1